3rd AIAA Atmospheric Space Environments Conference
27 - 30 June 2011, Honolulu, Hawaii

AIAA 2011-3150

RF Signatures of Hypervelocity Impacts on Spacecraft

Sigrid Close[1]
Stanford University, Stanford, CA, 94305

Michael C. Kelley[2]
Cornell University, Ithaca, NY, 14853

Alex Fletcher[3], Nicolas Lee[4]
Stanford University, Stanford, CA, 94305

and

Patrick Colestock[5]
Los Alamos National Laboratory, Los Alamos, NM, 87545

We investigate the radio frequency (RF) signature resulting from a hypervelocity impact on a spacecraft. While hypervelocity impactors, consisting of meteoroids, dust and orbital debris, are known to cause mechanical damage to satellites, very little is understood about the electrical effects associated with an impact. We present a theory to describe the behavior of the plasma produced from a hypervelocity impact, which results from ionization of both the particle as well as a small part of the spacecraft. The plasma, which does not penetrate the spacecraft chassis, produces a strong electromagnetic pulse (EMP) at a broad frequency spectrum, which can produce electrical anomalies or even catastrophic damage depending on the amount of electrical shielding. We compare our theory to data taken by the Cassini spacecraft in order to understand the resulting RF signature. Our analyses show that RF emission should be a routine outcome from impacts by particles but may only cause anomalies or failures when the impactor exceeds a velocity of 12 km/s.

I. Introduction

Spacecraft are subjected to a variety of space environment conditions that can cause minor to catastrophic anomalies. Many of these anomalies are attributed to space weather effects, such as proton, electron and cosmic ray impacts primarily originating from the sun. A subset of the anomalies are attributed to macroscopic, hypervelocity impacts associated with human-made orbital debris and natural meteoroids and dust. Although satellite owners and operators routinely classify and track anomalies, there is currently no centralized database that allows one to search for a clear, definitive cause for a satellite upset or failure. In many cases, it is not even possible to identify the definitive cause for a given anomaly despite the best efforts of spacecraft operators and manufacturers. Consequently, the relative contribution from all of these environmental causes is currently unknown.

While it is clear that debris, meteoroids and dust can cause mechanical damage to a spacecraft by penetrating the outer layer, it is unknown how or how often these macroscopic particles can cause electrical damage, whether or not penetration occurs. In particular, both electrostatic discharges (ESDs) and electromagnetic pulses (EMPs) have been loosely correlated to macroscopic impacts. Such instances include the Olympus communication satellite failure, that occurred during the peak of the Perseid meteor shower in 1993.[1] Olympus suffered a loss of gyro stability, which resulted in a complete loss of the satellite due to expenditure of fuel. In 2009, the Landsat-5 satellite suffered a similar anomaly also during the peak of the Perseid shower, but was able to recover. In 2004, the Jason-1 satellite

[1] Assistant Professor, Department of Aeronautics and Astronautics, Stanford University, Member AIAA.
[2] Professor, School of Electrical and Computer Engineering, Cornell University.
[3] Ph.D. Candidate, Department of Aeronautics and Astronautics, Stanford University, Student Member AIAA.
[4] Ph.D. Candidate, Department of Aeronautics and Astronautics, Stanford University, Student Member AIAA.
[5] Technical Staff, Los Alamos National Laboratory.

noted a momentum transfer, which resulted in a 30 cm change in its semimajor axis; this impact was followed by power spikes that occurred over the next 5 hours. The Olympus and Landsat cases suggest that electrical anomalies can result from hypervelocity impacts by very small particles, even when no penetration or mechanical damage occurs, while the Jason-1 anomaly suggests that impacts of larger particles can also result in an electrical effect.

In this paper, we investigate how hypervelocity impacts can create EMP and associated radio frequency (RF) emission in order to understand a potential mechanism for satellite anomalies and failures. We present a basic EMP model, followed by RF data recorded by the Cassini spacecraft, in order to understand how the emitted power changes as a function of frequency.

II. Plasma Model

The plasma model, which has been previously published[2], will be reviewed here for completeness. We begin with a general theory of plasmas formed by hypervelocity particle impacts on spacecraft. When the particle impacts the spacecraft, it ionizes itself as well as a small portion of the spacecraft producing a net charge, q. To address charge production, we model a particle impacting a spacecraft with a speed that can range from 4 to 80 km/s, which represents velocities associated with human-made debris as well as dust and meteoroids that reside in Solar orbit. We use an empirical formula to determine the charge production as a function of the impactor's mass and velocity based on ground-based measurements. Unfortunately, most of these ground-based measurements cannot reproduce what may be a typical impact condition for naturally occurring particles (≤ 1 μg traveling 60 km/s). However, these experiments have led to a generalized formula for charge production,[3] which is given by

$$q = 0.1m\left(\frac{m}{10^{-11}}\right)^{0.02}\left(\frac{v}{5}\right)^{3.48}, \tag{1}$$

where q is the total charge in C, m is the particle mass in g, and v is the meteoroid impact velocity in km/s. There are many variations of Equation 1 published in the literature[4,5,6] with speed exponents that range between 2.5 and 4.7. The chemical composition of the particle, as well as the type and charge of the target material, will affect the plasma production process. Additionally, the plasma produced may be multiply ionized with velocity coefficients that vary depending on primary or secondary ionization. The charge produced as a function of mass and velocity using Equation 1 is shown in Figure 1 for masses ranging from 10^{-21} to 10^{-6} g and for velocities between 4 and 80 km/s.

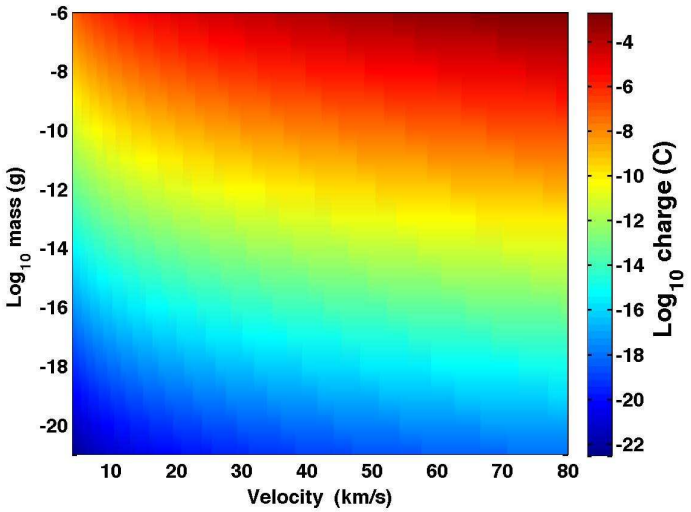

Figure 1. Charge (in coulombs) produced by a particle after impact with a spacecraft, as a function of particle mass and velocity.

We assume that the electrons become collisionally uncoupled from the bulk plasma and that the inherent electron oscillations are determined primarily by the local plasma frequency and bounded by the electron thermal velocity. It is these plasma oscillations in the sheath, which we describe as coherent in nature, that we wish to model to produce an estimate of the resulting EMP. When the initial plasma has diluted to the point where the electron-ion collision frequency is approximately equal to the plasma frequency, the surface electrons can effectively separate from the background ions and produce coherent radiation at the plasma frequency. The plasma expands freely, which lowers the density and the effective peak emission frequency; we assume that both the ion and electron temperature, however, are equal and frozen after this point in time, since no energy is exchanged with an external system. If the plasma is radiating, some energy will be lost. However, the amount is relatively insignificant in the first instances after the plasma begins to expand. For this reason, we assume the temperature is constant throughout the expansion process. This assumption will be relaxed in future models.

From this model, we can find the radiated power of the coherent oscillations, whereby a percentage of the electrons are oscillating in phase. For simplicity, we assume that a spherically symmetric charge distribution, q, results at the surface of the plasma. The bulk plasma expands at approximately the ion isothermal speed, c_s, and thus the plasma density decreases with distance and time according to

$$n_e(t) = \frac{n_{e,0}}{\left(1 + c_s t / r_0\right)^3}, \tag{2}$$

where

$$c_s = \sqrt{\frac{\gamma k T_e}{m_i}}, \tag{3}$$

and γ is the ratio of specific heats, $n_{e,0}$ is the initial plasma density at the initial radius, r_0, and t is time. The falloff of plasma density is plotted in Figure 2 for a given initial plasma density.

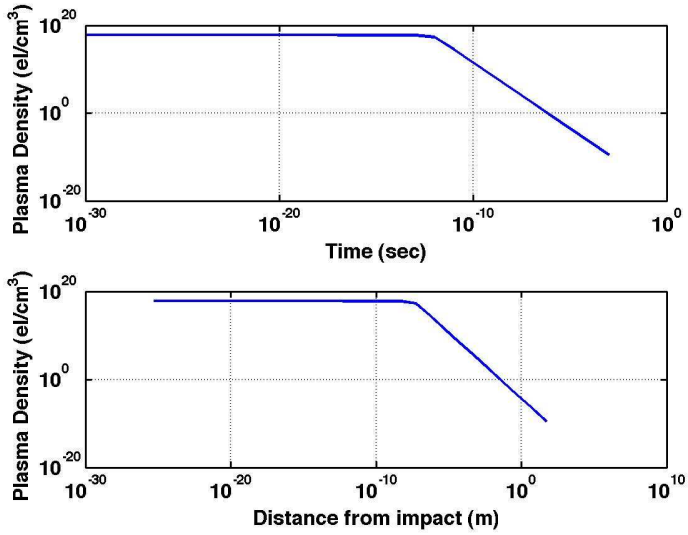

Figure 2. Plasma density as a function of time and distance from point of impact.

We can invoke a slab model of the expanding plasma and describe the relative displacement between the electrons and ions in the expanding plasma as $\xi(t) = r(t) - c_s t$. The power radiated by the coherent oscillations is computed from just the restoring field and equation of motion, which are, respectively,

$$E = -\frac{en_e\xi(t)}{\varepsilon_0}, \tag{4}$$

and

$$\ddot{\xi}(t) = -\frac{e^2 n_e \xi(t)}{m_e \varepsilon_0} = -\frac{\omega_{p,0}^2 \xi(t)}{\left(1 + c_s t / r_0\right)^3}, \tag{5}$$

where the peak plasma frequency is given by

$$\omega_{p,0}^2 = \frac{n_{e,0} e^2}{m_e \varepsilon_0}. \tag{6}$$

The boundary conditions are such that $\xi(0) = 0$ and $\dot{\xi}(0) = v_{th,e}$. The general solution to this equation is

$$\xi(t) = c_1 \frac{c_s}{2r_0}\left(1 + \frac{c_s t}{r_0}\right)^{1/2} J_1\left(\omega_{p,0}\frac{2r_0}{c_s}\left[1 + \frac{c_s t}{r_0}\right]^{-1/2}\right) + c_2 \frac{c_s}{2r_0}\left(1 + \frac{c_s t}{r_0}\right)^{1/2} Y_1\left(\omega_{p,0}\frac{2r_0}{c_s}\left[1 + \frac{c_s t}{r_0}\right]^{-1/2}\right), \tag{7}$$

where J_1 and Y_1 are the first order Bessel functions of the first and second kind, respectively, and c_1 and c_2 are constants satisfying the initial conditions. Using Equation 7, we can plot the time from impact as a function of the displacement between the electrons and ions as a function of time from impact. This is shown in Figure 3 and displays the oscillatory behavior of the electrons with respect to the ion boundary as the plasma expands. These results were generated using a microgram-sized particle impacting at 50 km/s.

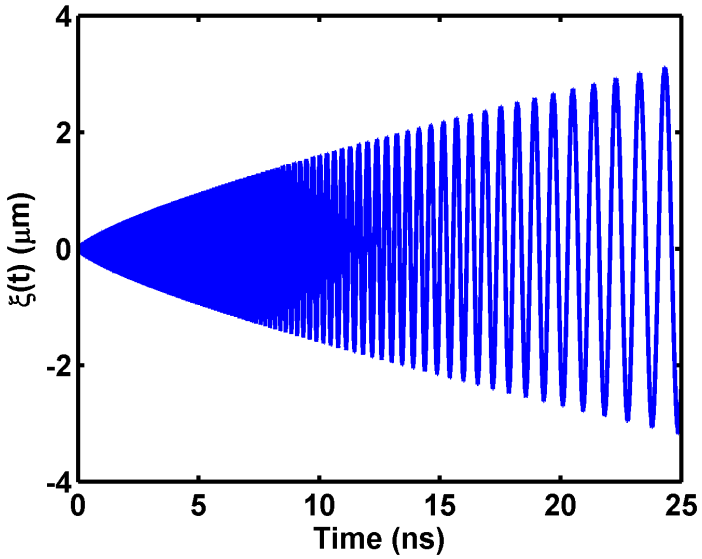

Figure 3. Plot of coherent electron oscillations about the expanding ion front for a 50 km/s impact of a microgram-sized particle

The total radiated power is found from the familiar Larmor formula, where we have used the WKB solution to the equation of motion to substitute for $|\dot{v}|^2$:

$$P = \frac{\omega_{p,0}^4 \left(\frac{v_{th,e}}{\omega_{p,0}}\right)^2 e^2 N \sin^2\left(\omega_{p,0}\frac{r_0}{c_s}\left[1+\frac{c_s t}{r_0}\right]^{-1/2}\right)}{6\pi e_0 c^3 \left(1+\frac{c_s t}{r_0}\right)^{9/2}}, \tag{8}$$

where N is the number of electrons involved in the motion. Fourier analyzing the above expression leads to the spectrogram, as shown in Figure 4. These results were generated using the same impact parameters as above (a microgram-sized particle impacting at 50 km/s).

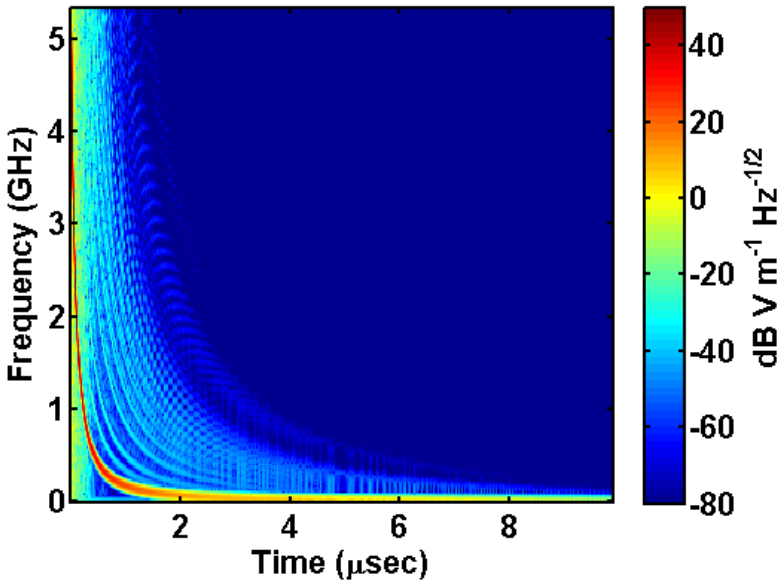

Figure 4. Spectrogram of the emitted power, showing a chirp with oscillatory behavior.

III. Data from Cassini RF Measurements

In order to compare our theory to data, we use impacts collected by the Radio and Plasma Wave Science (RPWS) experiment on Cassini.[7,8] These data correspond to impacts from dust stream particles[9] on the high-gain antenna dish, and include broadband electric field measurements from the 10 m dipole antennas on Cassini. For these impact events, where the particles are traveling at approximately 450 km/s, we are able to analyze the complete waveform (up to 110 kHz). For one representative impact event, these data are shown in Figure 3 and include the temporal waveform (top panel), a discrete Fourier analysis (middle panel), and a wavelet analysis (bottom panel). The top panel shows an ESD pulse with an amplitude of 25 microvolts. This is immediately followed by what appears to be oscillations that decay with time. The middle panel shows a discrete Fourier analysis of these data for different segments of time and also indicates an oscillatory behavior. The spectrum

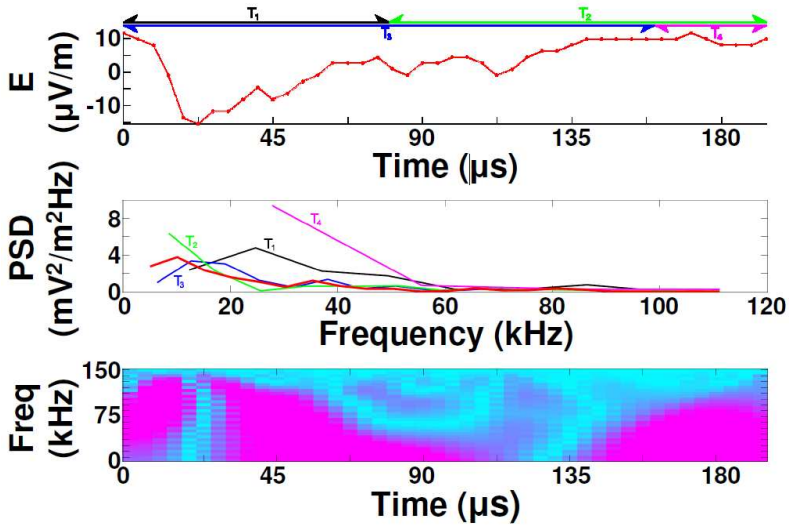

Figure 5. Waveform, discrete Fourier analysis and wavelet analysis associated with impacts from nanometer-sized particles at solar wind velocity (450 km/s), as detected by Cassini's RPWS dipole antennas.

indicated in red is the discrete Fourier transform of the entire waveform of 200 microseconds. Each of the other discrete Fourier transforms is colored and labeled to correspond with the time intervals indicated on the top panel (T_1 through T_4). The bottom panel shows a wavelet analysis, revealing an initial broadband pulse correlating to wavelets that span all 32 frequency bins. Then, the wavelet signals occur at the highest frequencies and progress to the lowest frequencies. This wavelet structure suggests a chirp-like signal that decreases in time – consistent with the model described in the previous section.

IV. Conclusion

We have described a possible mechanism for RF signatures associated with hypervelocity impacts on spacecraft. In particular, we have put forth a model that characterizes the EMP that may be produced upon impact. The low-frequency peak in the emission spectrum indicates that spacecraft components sensitive to VLF or lower bands, as well as S-band frequencies, are especially vulnerable to electrical effects from EMP. The rapid dissipation of the plasma indicates that any electrical effect from a hypervelocity impact will be localized and that there will be very little effect beyond its immediate vicinity.

Our future work will address inclusion of a background ionosphere that is applicable to low-earth-orbiting satellites and may allow for momentum exchange through a wave mechanism, as well as inclusion of a background magnetic field that may play a role at later, lower frequencies. We will also examine the role of dust formation post impact in order to assess whether electron attachment can reduce the expansion velocity by cause a macroscopic charge separation[10] and model different target materials (such as solar cells). We plan to develop a particle-in-cell simulation in order to relax many of the simplifying geometric assumptions used in the presented model. This work will be complemented by experimental ground testing at a hypervelocity impact facility in order to validate the model, followed by a proposed CubeSat mission to provide direct measurements of RF emission from meteoroid impacts.

Acknowledgments

The authors gratefully acknowledge the contributions from Stan Green.

References

[1]Caswell, R. D. et al., Olympus end of life anomaly – a perseid meteoroid impact event?, *Int. J. Impact Engng*., vol. 17, pp. 139-150, 1995.

[2]Close, S., P. Colestock, L. Cox, M. Kelley and Nl. Lee, Electromagnetic pulses generated by meteoroid impacts on spacecraft, *JGR*, vol 115, 2010.

[3]Drolshagen, G., Impact effects from small size meteoroids and space debris, *Adv. Space Res*., vol. 41, pp. 1123–1131, 2008.

[4]Ratcliff, P. R. et al., Velocity thresholds for impact plasma production, *Adv. Space Res.,* vol. 20, pp. 1471-1476, 1997a.

[5]Ratcliff, P. R. et al., Experimental measurements of hypervelocity impact plasma yield and energetics, *Int. J. Impact Engng*., vol. 20, pp. 663-674, 1997b.

[6]McDonnell, T. and P. R. Ratcliff, Investigation of energy partitioning in hypervelocity impacts, Final Report, USAF/EOARD Research Contract F61708-95-C0011, 1996.

[7]Z. Wang, D.A. Gurnett, T. F. Averkamp, A. M. Persoon, and W. S. Kurth, "Characteristics of dust particles detected near Saturn's ring plane with the Cassini Radio and Plasma Wave instrument," *Planet. Space Sci.,* vol. 54, no. 9-10, pp. 957-966, Aug. 2006.

[8]N. Meyer-Vernet, A. Lecacheux, M. L. Kaiser, and D. A. Gurnett, "Detecting nanoparticles at radio frequencies: Jovian dust stream impacts on Cassini/RPWS," *Geophys. Res. Lett.,* vol. 36, no. 3, L03103, doi:10.1029/2008GL036752, Feb. 2009.

[9]Kempf, S., Srama, R., Horányi, M., Burton, M., Helfert, S., Moragas-Klostermeyer, G., et al. High-velocity streams of dust originating from Saturn. *Nature* vol. 433, no. 7023, pp. 289-291, 2005.

[10]Crawford, D. A. and P. H. Schultz, Electromagnetic properties of impact-generated plasma, vapor, and debris, *Int. J. Impact Engng*., vol. 23, pp. 169-180, 1999.